Hydrodynamics of Permeable Horseshoe Obstacle in Fluvial Environment: A Physical Modelling

H. Chanson
The University of Queensland, h.chanson@uq.edu.au

H. K. Lee
The University of Queensland

W. Johnson
The University of Queensland

Recommended Citation

Chanson H., Lee, H.K., and Johnson, W. (2022). "Hydrodynamics of Permeable Horseshoe Obstacle in Fluvial Environment: A Physical Modelling" in "9th IAHR International Symposium on Hydraulic Structures (9th ISHS)". *Proceedings of the 9th IAHR International Symposium on Hydraulic Structures – 9th ISHS*, 24-27 October 2022, IIT Roorkee, Roorkee, India. Palermo, Ahmad, Crookston, and Erpicum Editors. Utah State University, Logan, Utah, USA, 10 pages (DOI: 10.26077/d9ec-010f) (ISBN 978-1-958416-07-5).

9th International Symposium on Hydraulic Structures Roorkee, India 24-27 October 2022
ISBN: 978-1-958416-07-5 DOI: https://doi.org/10.26077/d9ec-010f

Hydrodynamics of Permeable Horseshoe Obstacle in Fluvial Environment: a Physical Modelling

H. Chanson[1], H.K. Lee[1] & W. Johnson[1]
[1]*The University of Queensland, School of Civil Engineering, Brisbane, Australia*
E-mail: h.chanson@uq.edu.au

Abstract: *Along Australian inland waterways, a number of man-made horseshoe obstacles were built for centuries. The permanent structures interacted with the streamflow across a wide range of water discharges including when they are fully-submerged. Their use ranged from water holes and fish trap at low to moderate flows, to large bed roughness and turbulent manipulation at large water discharges. The aim of the study was to gain a sound physical understanding of the hydraulic operation of horseshoe obstacle across a broad range of submergence ratio, ranging from low flows and emergent obstacle to major floods with fully-submerged structures. In this laboratory study, the physical modelling of permeable horseshoe obstacle was undertaken under controlled flow conditions, based upon a Froude similitude. Two physical models were built corresponding to a 5:1 and 20:1 geometric scaling ratio for typical riverine structures. The scale models were 3D-printed with random pattern and a porosity of 0.27, close to the porosity of rockfill material. The physical observations included visual observations, three-dimensional free-surface profiles and detailed velocity measurements. The physical observations showed a broad range of flow patterns, depending upon the submergence ratio. The porosity of the obstacle facilitated some interactions between the seepage and recirculation region, leading to changes in the wake region and its turbulence, compared to a impervious obstacle with the same shape.*

Keywords: *Physical modelling; Horseshoe obstacle; Wake region; Riverine interactions.*

1. Introduction

Along inland Australian waterways, indigenous Australians built hydraulic structures over a long period time, and there are a wide variety of waterworks (Bandler 1995, 2003). One type of structure was the rock fish trap (Mathews 1903, Flecker 1951, Dargin 1976, Bandler 2007). Although a wide range of shapes were in usage, a common shape was a horseshoe element opened downstream. Most structures were built of stones set and key without mortar or clay (Dargin 1976). The porous construction facilitated the resistance to the current and prevented siltation during floods. The permanent structures have interacted with the fluvial flow for a broad range of flow rates over log period of times, including when the elements were fully-submerged. Plates and photographs suggested that the rock fish traps were used pro-actively for fishing when the water levels were less than waist height (Fig. 1) (Dargin 1976). The constraint derived directly from the stability and safety of the fishermen/women in the river waters, since higher water depths would prevent their ability to stand, move and fish in the riverine environment (Takahashi et al. 1992, Xia et al. 2014, Chanson and Brown 2018). For other flow conditions, the horseshoe elements could retain water in the trap and rock holes during dry periods, contributing to groundwater recharge and creating drinking holes for fauna. During large flows, the structures interacted with the flood flow, generating strong secondary motion.

At low flows, the operation of horseshoe structures presents some similarity with the overflow of horseshoe waterfalls (Pasternack et al. 2006,2007, Lapotre and Lamb 2015) and man-made horseshoe weirs (Stamataki et al. 2014). At high flows, the fluid flow around the horseshoe fish trap exhibits some analogy with atmospheric boundary layer flows past canopy patches (TaddeiI et al. 2016) and past shallow islands (Branson et al. 2019). The obstacle porosity plays a key role, affecting the wake flow, reducing the total drag on the structure and the risks of downstream scour (Wüthrich et al. 2020, Gillies et al. 2021). Yet, the literature on the hydrodynamic of porous horseshoe structure is nil.

The aim of the study was to gain a sound physical understanding of the hydrodynamics of porous horseshoe obstacle in rivers, across a broad range of submergence ratio. The physical investigation covered a broad range of conditions, from low flows and emergent obstacle to major floods with fully-submerged structures. The physical modelling of permeable horseshoe obstacle was undertaken under controlled flow conditions, based upon a Froude similitude with a 5:1 and 20:1 geometric scaling ratio for a typical riverine structure.

Figure 1. Historic (probably posed) photo of a man fishing in the Brewarrina Aboriginal rock fish traps / Baiame's Ngunnhu, published in The Dawn 1893 - Main flow direction from bottom right to top left.

2. Physical modelling, facility and instrumentation

New experiments were performed in two 3.2 m long 0.4 m wide channels and a 15 m long 0.5 m wide channel located in the AEB Hydraulics Laboratory of The University of Queensland (Australia). In each flume, the test section consisted of smooth PVC bed and glass walls. The bed slope was horizontal and the waters were supplied by a constant head tank. In one 0.4 m wide channel, the flow rates were recorded with a volume per time technique, well-suited for small to medium flows. In the other 0.4 m wide flume, the discharges were measured with an orifice meter installed along the supply line connected the reticulation system of the laboratory. In the 0.5 m wide flume, the flow rates were recorded with a Venturi meter. The water depths were recorded with pointer gauge. Velocity measurements were undertaken with a Dwyer® 166 Series Prandtl-Pitot tube with a 3.18 mm diameter tube made of corrosion resistant stainless steel, featuring a hemispherical total pressure tapping (Ø = 1.19 mm) at the tip and four equally spaced static pressure tappings (Ø = 0.51 mm) located 25.4 mm behind the tip. The tip design met AMCA and ASHRAE specifications and the tube did not require calibration. Additional measurements were conducted with a total head tube (Ø = 0.915 mm). The translation of the velocity probes in the vertical direction was controlled by a fine adjustment travelling mechanism connected to a HAFCO^{TM} digital scale unit. Flow visualisations using dye injection were conducted with digital cameras, operating in movie mode at 120 fps, 100 fps and 30 fps.

Table 1. Horseshoe structure model characteristics

Reference	Height h (m)	Outer diameter D (m)	Annular thickness t (m)	Porosity	Comment
L4	0.089	0.174	0.034	0.27	Random pattern
M4	0.051	0.100	0.020	0.27	Random pattern
M3				0.29	8mm hole lattice
M2				0.64	4mm hole lattice
M1				0	Plain

Table 2. Experimental test conditions

Channel	S_o	Width B (m)	Discharge measurement technique	Discharge Q (m^3/s)	x_o (m)	Horseshoe structure model	Instrumentation
B	0	0.5	Venturi meter	0.01-0.10	8.16	L4	Pointer gauge, Prandtl-Pitot tube, total head tube
2		0.4	Orifice meter	0.010-0.05	1.185	M1 to M4	Pointer gauge
1			Volume per time	0-0.012	1.185	M1 to M4	Pointer gauge

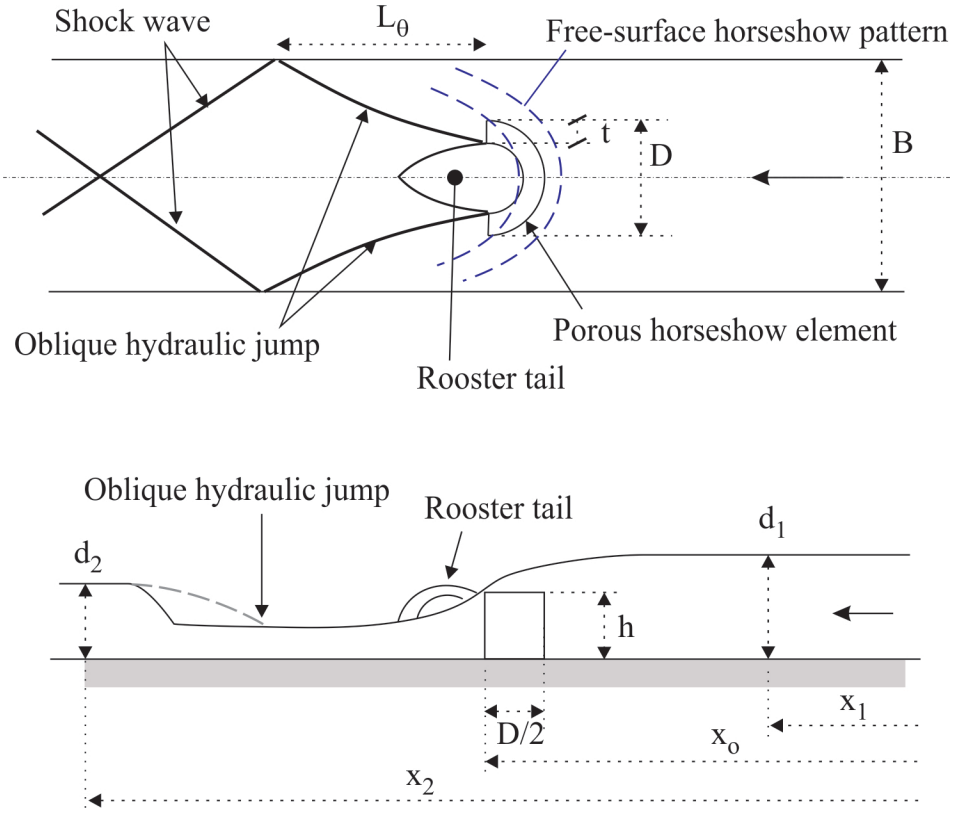

Figure 2. Definition sketch of the flow past a submerged porous horseshoe element ($d_1/H \sim 1,2\text{-}1,3$) in channels 1 & 2.

The rock fish traps were modelled with simple semi-circular horseshoe elements (Table 1). The selection of the two model sizes was mostly related to the measurement techniques. Initial tests in the small-size facility provided detailed information on the free-surface patterns. The large-size facility was used to undertake velocity measurements, with minimum blockage and impact of the Pitot tube. Since most Australian indigenous rock fish traps were between 0.5 m and 1 m high (Fig. 1), the two models corresponded to 5:1 down to 20:1 geometric scale models. The models were 3D printed out of a resin with density 1164.2 kg/m^3. A metallic plate was attached to the footing of each model, and attached to the flume invert with a magnetic strip. The elements were placed on the channel centreline. All the experiments will be conducted with zero bed slope, and the downstream gate was fully-opened, i.e. no tailwater effect. The flow conditions are summarised in Table 2 and a definition sketch is presented in Figure 2.

3. Free-surface flow patterns

The free-surface flow patterns were investigated in the three flumes for all flow conditions (Table 2), although a greater focus was given for inflow conditions such that $0.4 < d_1/h < 2$ with d_1 the inflow depth and h the vertical height of the element.

With the horseshoe element being partially-submerged, the upstream free-surface developed a horseshoe surface pattern when critical flow conditions took place around the element. This three-dimensional surface pattern is illustrated in Figure 3. A strong recirculation took place in the near-wake of the element. With the porous elements (Fig. 3A & 3B), the recirculation was fed by the seepage through the element, leading to a more stable and relatively less intense recirculation region, than for the impervious model (Fig. 3C). Interestingly, Wũthrich et al. (2020) observed a similar surface pattern around an un-submerged rectangular building.

When the upstream flow depth was about the height of the element, some difference in flow pattern was seen between the impervious model (M1) and the porous models. With the impervious element, the overflow above the element top plunged into the recirculation and modified the wake region. This was observed for $1 < d_1/h < 1.2\text{-}1.3$. Such an overflow-recirculation was not observed with the porous elements, with a more gentle flow pattern transition from partially-submerged to fully-submerged element.

When the horseshoe element was fully-submerged, a marked horseshoe free-surface pattern was observed and shock waves separated from the element and propagated downstream (Fig. 4). At very large flow rates ($d_1/h > 2.5$), the element no longer interacted with the free-surface and acted as an isolated roughness patch

The impact of the horseshoe element on the flow was tested by systematically recording the water depths along the channel, with and without element. The inflow depth d_1 was consistently measured at $(x_1\text{-}x_o)/h = -5$ and the downstream depth d_2 at $(x_2\text{-}x_o)/h = +25$, with x_o the longitudinal location of the element (Fig. 2). Both depths were recorded on the channel centreline. Although the accuracy on the inflow depth was within ±0.5 mm, the error on the downstream depth data was larger because of the three-dimensional flow patterns, e.g. shock waves, hydraulic jumps (Figs. 2, 3 & 4). Typical results are presented in Figure 5, in terms of the dimensionless inflow depth d_1/h and dimensionless differences in water depths $(d_1\text{-}d_2)/h$.

Overall, the data showed a number of key observations. First, the presence of the horseshoe element increased the upstream depth, compared to the channel without element, for the same flow rate and channel (Fig. 5A). Second, the inflow depth d_1 was with the plain (M1), impervious element than with the porous elements (M2, M3, M4) for the same flow rate (Data not shown). The finding implied that the porous elements generated lesser flow resistance and associated energy dissipation. Third, some differences in terms of the dimensionless inflow and downstream depths, d_1/h and d_2/h, were observed between the porous elements L4 and M4, designed with the same porosity (Fig. 5B). While the difference was small in terms of the upstream depth, the data in terms of $(d_1\text{-}d_2)/h$ was much larger, This is seen in Figure 5 B for $d_c/h > 0.7$ and $d_1/h > 1$. Such differences were likely linked to (a) the different channel breadths B/h: i.e., B/h = 5.6 and 8 for the small and large channels respectively, ad (b) some difference in tailwater conditions, with a marked hydraulic jump seen in the larger channel downstream of model L4.

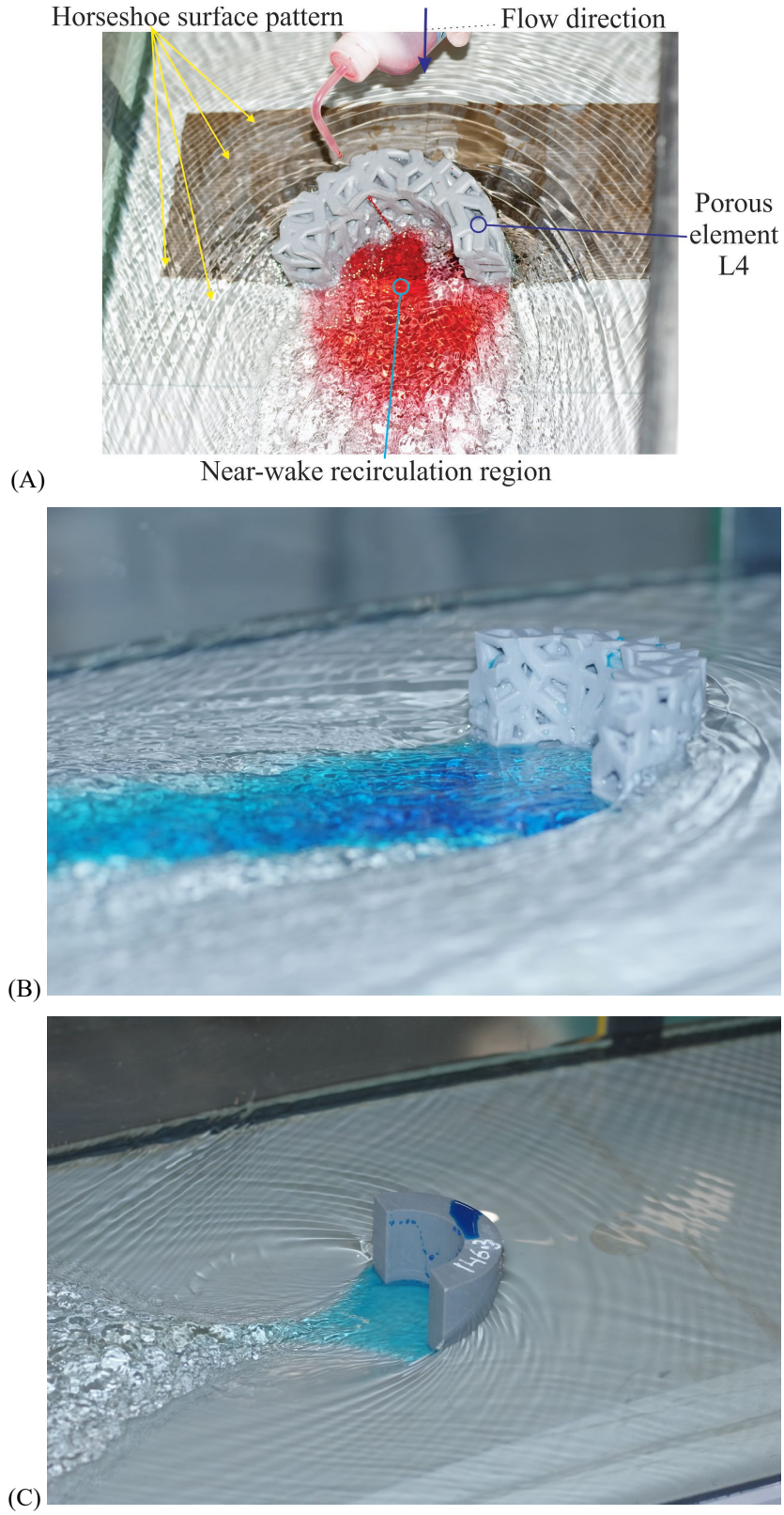

Figure 3. Flow patterns around a partially-submerged horseshoe element with $d_1/H \sim 0.75$. Dye injection highlights the near-wake recirculation region. (A) Model L4, $d_1/H = 0.725$, $Q = 0.012$ m^3/s; (B) Model M4, $d_1/H = 0.77$, $Q = 0.0042$ m^3/s; (C) Model M1, $d_1/H = 0.74$, $Q = 0.0040$ m^3/s.

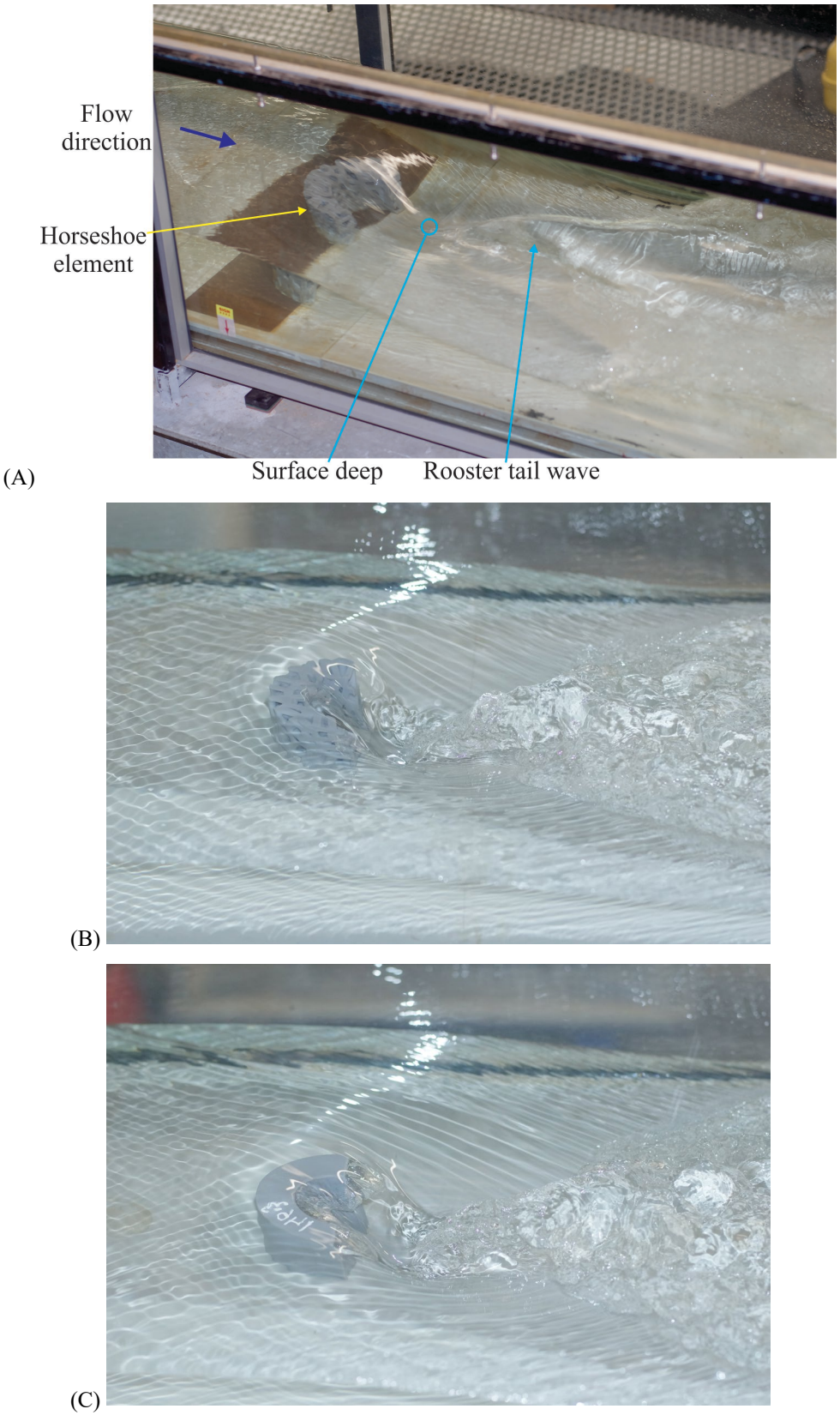

Figure 4. Flow patterns around a fully-submerged horseshoe element for $d_1/H \sim 1{,}4$. (A) Model L4, $d_1/H = 1.445$, $Q = 0.0447$ m^3/s; (B) Model M4, $d_1/H = 1.38$, $Q = 0.0121$ m^3/s; (C) Model M1, $d_1/H = 1.4$, $Q = 0.0128$ m^3/s.

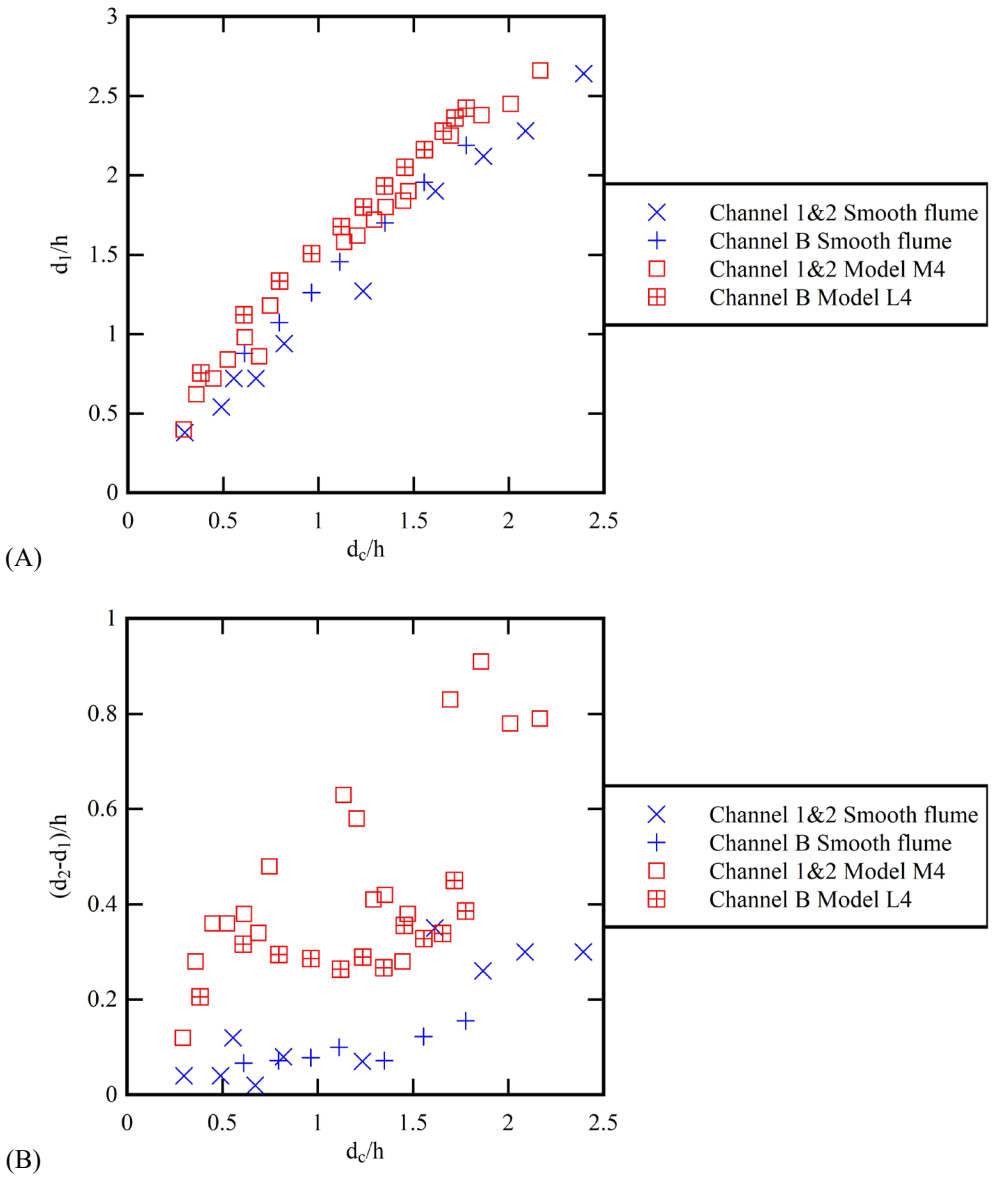

Figure 5. Impact of the porous horseshoe elements L4 and M4 (Porosity: 27%) on the inflow depth and difference in flow depths. (A) Dimensionless inflow depth d_1/h as a function of the dimensionless discharge d_c/h; (B) Dimensionless decrease in flow depth $(d_1-d_2)/h$ as a function of the dimensionless discharge d_c/h.

4. Velocity measurements

Pressure and velocity measurements were conducted in the larger channel B with the large porous element model L4, seen in Figures 3A and 4A. While the large majority of the data were collected with the Prandtl-Pitot tube, a smaller total head tube was used in regions where the streamline direction deviated from the channel centreline, as well as in the near-wake of the element. Typical velocity data are presented in Figures 6 and 7.

First, the pressure measurements showed that the pressure gradient was hydrostatic at all measurement locations. Overall, the streamline curvature was small in the entire flow field, except possibly at the downstream edges of the semi-circular element, where the pressure could not be measured locally with the Prandtl-Pitot tube.

Second, the velocity measurements showed that the inflow conditions were partially developed. The approach flow around the horseshoe element presented a streamline pattern in agreement with irrotational flow theory of ideal fluid,

e.g. similar to the streamline pattern around a circular cylinder for $(x-x_o) < 0$ (Rouse 1959, Vallentine 1969, Chanson 2014). Downstream of the horseshoe element, the supercritical flow interacted with the recirculation region, with two marked shear zone, seen in Figure 6. Figure 6A presents a typical transverse distribution of the longitudinal velocity. A marked velocity gradient $\partial V_x/\partial y$ is observed at y±D/2. Figure 7 illustrates the major change in velocity filed around the porous horseshoe element. Figure 7 shows velocity contour maps in the accelerating flow region around the element (Fig. 7A) and immediately downstream of the horseshoe element (Fig. 7B).

Third, some negative velocity was observed in the recirculation zone. While the Prandtl-Pitot tube was not designed to measure negative velocities, a lower reading in the dynamic tapping was observed, compared with the static tube, at these locations. In addition, dye injection confirmed qualitatively the observations. Past studies derived a correlation between the negative Pitot reading and negative velocity (Cabonce et al. 2019). Although the quantitative magnitude was questionable in the current study, the findings could not be ignored, as reported in Figure 7B.

Overall, the velocity measurements highlighted a complicated three-dimensional velocity field around the porous horseshoe element.

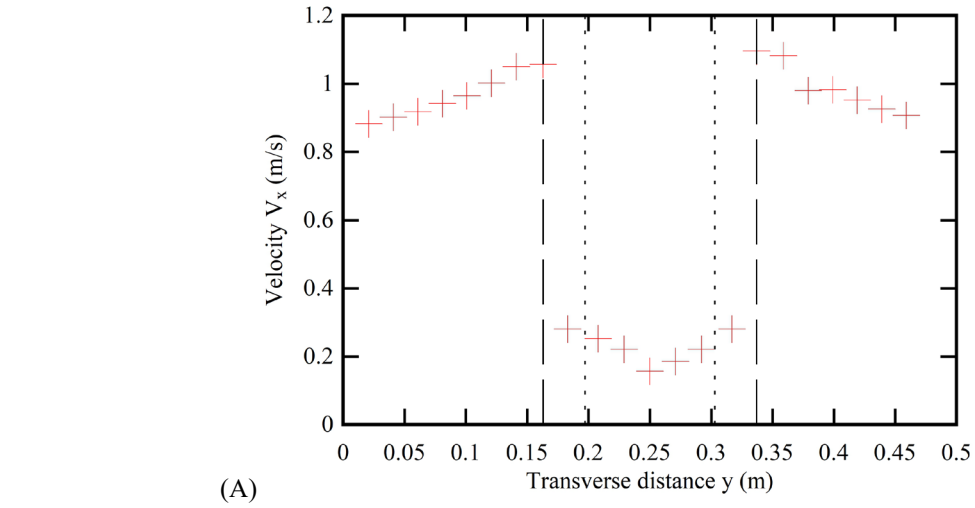

Figure 6. Transverse profile of longitudinal velocity at $(x-x_o) = 0.050$ m and z = 0.025 m for Q = 0.020 m^3/s, $d_1 = 0.10$ m, porous Model L4 (Channel B). Dashed and dotted black mark the downstream edges of the horseshoe element. (A) Velocity profile; (B) Photographs of the flow.

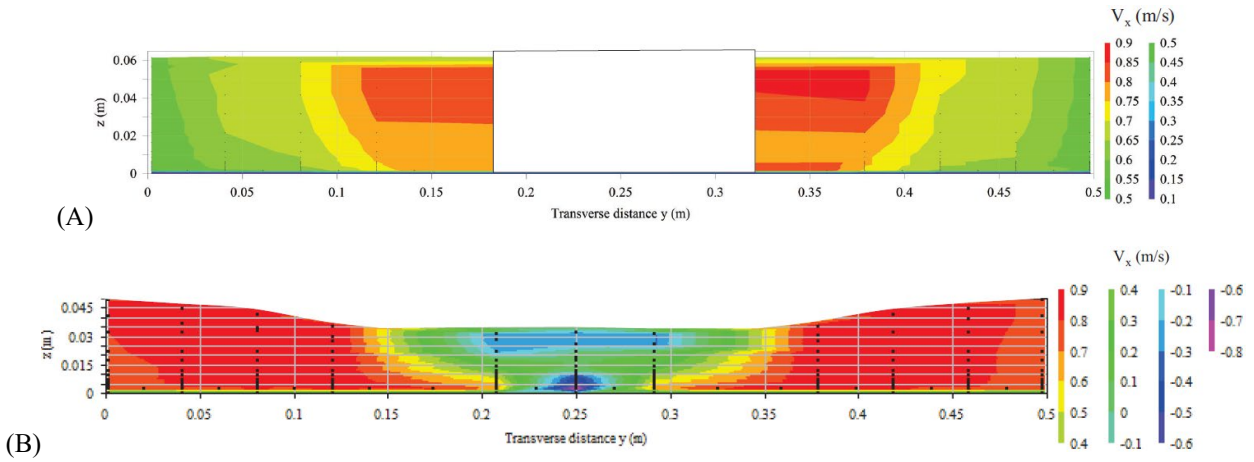

Figure 7. Un-distorted velocity contour maps for Q = 0.012 m^3/s, porous Model L4 (Channel B). (A) $(x-x_o)$ = -0.050 m; (B) $(x-x_o)$ = +0.050 m.

5. Conclusion

A physical study of horseshoe obstacles was undertaken, to gain a greater understanding of man-made structures built along Australian inland waterways for centuries. The physical modelling of permeable horseshoe obstacle was undertaken under controlled flow conditions, based upon a Froude similitude at two scales, corresponding to between 5:1 and 20:1 for typical riverine structures. The scale models were 3D. The physical observations included visual observations, three-dimensional free-surface profiles and detailed pressure and velocity measurements.

The physical observations showed a broad range of flow patterns, depending upon the submergence ratio. The porosity of the obstacle facilitated some interactions between the seepage and recirculation region, leading to changes in the wake region and its turbulence, compared to a impervious obstacle with the same shape. The velocity measurements presented a complicated three-dimensional velocity field around the porous horseshoe element, with an accelerating flow motion as the flow divides around the obstacle, followed by complicated three-dimensional flow patterns downstream of the elements

The present work paves the way for more detailed studies of real-life prototype structures Further investigations should test the impact of adjacent horseshoe structures (e.g. Fig. 1), different tailwater conditions, the interactions with aquatic life, as well as sediment processes.

6. Acknowledgments

The first author acknowledges some helpful exchanges with Dr Duncan Keenan-Jones (UQ School of Historical and Philosophical Inquiry), Sarah Martin, and Dr Michael Westaway (UQ School of Social Sciences) in alphabetical listing. The financial support of the University of Queensland, School of Civil Engineering is acknowledged.

7. References

Bandler, H. (1995). "Water resources exploitation in Australian prehistory environment." *The Environmentalist*, Vol. 15, pp. 97-107.

Bandler, H. (2003). "Expertise in Finding Water and Exploiting Water Resources in Australian Prehistory." in "Wasserhistorische Forschungen. Schwerpunkt Antike", *Schriften der Deutschen Wasserhistorischen Gesellschaft (DWhG) e.V. Siegburg*, C. P. J. Ohlig Editor, pp. 81-96.

Bandler, H. (2007). "Expertise in finding water and exploiting water resources in Australian prehistory." *Australian Journal of Water Resources*, Vol. 11, No. 1, pp. 1-11.

Branson, P.M., Ghisalberti, M., and Yvey, G.N. (2019). "Three-dimensionality of shallow island wakes." *Environmental Fluid Mechanics*, Vol. 19, pp. 1393-1416 (DOI: 10.1007/s10652-019-09661-5).

Cabonce, J., Fernando, R., Wang, H., and Chanson, H. (2019). "Using Small Triangular Baffles to Facilitate Upstream Fish Passage in Standard Box Culverts." *Environmental Fluid Mechanics*, Vol. 19, No. 1, pp. 157–179 (DOI: 10.1007/s10652-018-9604-x)

Chanson, H. (2014). "Applied Hydrodynamics: An Introduction." *CRC Press*, Taylor & Francis Group, Leiden, The Netherlands, 448 pages & 21 video movies.

Chanson, H., and Brown, R. (2018). "Stability of Individuals during Urban Inundations: What Should We Learn from Field Observations?" *Geosciences*, Vol. 8, No. 9, Paper 341, 9 pages (DOI: 10.3390/geosciences8090341).

Dargin, P. (1976). "Aboriginal Fisheries of the Darling-Barwon Rivers." *Brewarrina Historical Society*, Brewarrina NSW, Australia, 77 pages.

Flecker, P.O. (1951). "Remains of Aboriginal Habitation on the Great Barrier Wall." *The North Queensland Naturalist*, Vol. 19, No. 97, pp. 1-3.

Gillies, J.A., McKenna Neumann, C., and O'Brien, P. (2021). "Flow around surface-mounted permeable cubes on solid and deformable surfaces." *Environmental Fluid Mechanics*, Vol. 21, pp. 619-641 (DOI: 10.1007/s10652-021-09789-3).

Lapotre, M.G.A., and Lamb, M.P. (2015). "Hydraulics of floods upstream of horseshoe canyons and waterfalls." *Journal of Geophysical Research Earth Surfaces*, Vol. 120, pp. 1227-1250 (DOI: 10.1002/2014JF003412).

Mathews, R.H. (1903). "The Aboriginal Fisheries at Brewarrina." *Journal and Proceedings of the Royal Society of New South Wales*, Vol. 37, pp. 146-156.

Pasternack, G.B., Ellis, C.R., Leier, K.A., Valle, B.L., and Marr, J.D. (2006). "Convergent hydraulics at horseshoe steps in bedrock rivers." *Geomorphology*, Vol. 82, pp. 126-145.

Pasternack, G.B., Ellis, C.R., and Marr, J.D. (2007). " Jet and hydraulic jump near-bed stresses below a horseshoe waterfall." *Water Resources Research*, Vol. 43, Paper W07449, 14 pages.

Rouse, H. (1959). "Advanced Mechanics of Fluids." *John Wiley*, New York, USA, 444 pages.

Stamataki, I., Zang, J., Bazeley, W.D., and Morgan, G.C.J. (2014). "Study of Flow Over Weirs such as Pulteney Weir." *Proc. 11th International Conference on Hydroscience & Engineering ICHE 2014*, Hamburg, Germany, Lehfeldt & Kopmann Editors, pp. 295-302.

Taddei, S., Manes, C., and Ganapathisubramani, D. (2016). "Characterisation of drag and wake properties of canopy patches immersed in turbulent boundary layers." *Journal of Fluid Mechanics*, Vol. 798, pp. 27-49 (DOI: 10.1017/jfm.2016.312).

Takahashi, S., Endoh, K., and Muro, Z.I., (1992). "Experimental Study on People's Safety against Overtopping Waves on Breakwaters." *Report on the Port and Harbour Institute*, Vol. 34, No. 4, pp. 4-31 (in Japanese).

Vallentine, H.R. (1969). "Applied Hydrodynamics." *Butterworths*, London, UK, SI edition.

Wüthrich, D., Pfister, M., and Schleiss, A.J. (2020). "Forces on buildings with openings and orientation in a steady post-tsunami free-surface flow." *Coastal Engineering*, Vol. 161, Paper 103753, 11 pages.

Xia, J., Falconer, R.A., Wang, Y., and Xiao, X. (2014). "New Criterion for the Stability of a Human Body in Floodwaters." *Journal of Hydraulic Research*, IAHR, Vol. 52, No. 1, pp. 93-104.